Comparative Proteomic Study of Retinal Ganglion Cells Undergoing Various Types of Cellular Stressors.

Christopher R. Starr and Marina S. Gorbatyuk

Department of Optometry and Vision Science, University of Alabama at Birmingham, Birmingham, Alabama, USA, 35233

*To whom correspondence should be addressed:
Dr. Marina S. Gorbatyuk.
Department of Optometry and Vision Science, School of Optometry,
University of Alabama at Birmingham.
1670 University Blvd., Birmingham, Alabama 35233.
Tel: 205- 934-6762. Fax: 205-934-3425.
Email: mgortk@uab.edu.

Abstract

Retinal ganglion cell (RGC) damage serves as a key indicator of various retinal degenerative diseases, including diabetic retinopathy (DR), glaucoma, retinal arterial and retinal vein occlusions, as well as inflammatory and traumatic optic neuropathies. Despite the growing body of data on the RGC proteomics associated with these conditions, there has been no dedicated study conducted to compare the molecular signaling pathways involved in the mechanism of neuronal cell death. Therefore, we launched the study using two different insults leading to RGC death: glutamate excitotoxicity and optic nerve crush (ONC). C57BL/6 mice were used for the study and underwent NMDA- and ONC-induced damages. Twenty-four hours after ONC and 1 hour after NMDA injection, we collected RGCs using CD90.2 coupled magnetic beads, prepared protein extracts, and employed LC-MS for the global proteomic analysis of RGCs. Statistically significant changes in proteins were analyzed using the Shiny Go program to identify GO biological processes and molecular functions resulting from the treatment. We identified unique and common alterations in protein profiles in RGCs undergoing different types of cellular stressors. Additionally, we observed the absence of certain proteins in treated RGCs compared to the control group. Our study not only identified both unique and shared proteomic changes but also laid the groundwork for the future development of a therapeutic platform for testing gene candidates for DR and glaucoma.

Keywords

Retina, Proteomics, Glaucoma, Excitoxicity, Optic Neuropathy, Opthalmology

1 Introduction

Retinal ganglion cells (RGCs) are neurons located in the retina of the eye, playing a crucial role in vision by transmitting visual information from the retina to the brain. There are several types of RGCs, each with a specific function in processing visual information. They receive input from photoreceptor cells, rods and cones, and integrate this information before sending it to the brain via the optic nerve. The axons of RGCs form the optic nerve, which carries visual signals to the brain, where signals are further processed to create the visual perception. Once damaged, axons of the mammalian central nervous system (CNS) fail to regenerate. RGCs are of clinical relevance in diabetic retinopathy (Abu-El-Asrar et al., 2004), glaucoma (Joo et al., 1999), retinal arterial and retinal vein occlusions (Sucher et al., 1997) as well as optic neuropathies (Khan et al., 2021). In these diseases, RGCs may be irreversibly damaged. It is widely accepted that damaged RGCs not only serve as a model of optic neuropathies but also as the primary model for studying mechanisms of CNS axon degeneration and how therapies may promote regeneration.

After insult, both intrinsic and extrinsic factors contribute to whether CNS neurons survive, retain, or regenerate their axons. Although lowering intraocular pressure (IOP) is an approved treatment for glaucoma, it is not effective for every patient, and many other diseases affecting CNS neurons lack approved treatment options. In glaucoma, it has been reported that RGCs undergo apoptosis triggered by various factors, including autophagy, glutamate neurotoxicity, oxidative stress, neuroinflammation, immunity, and vasoconstriction (Kuehn et al., 2005; Shen et al., 2023). Autophagy can be induced by retinal hypoxia and axonal damage (Shen et al., 2023) while glutamate neurotoxicity is induced by the overstimulation of N-methyl-D-aspartate membrane receptors by glutamate, leading to progressive glaucomatous optic neuropathy (Shen et al., 2023).

In diabetes, retinal neuropathy involves progressive RGC death, axonal degeneration, and consequently, optic nerve degeneration (Bikbova et al., 2014). RGC loss occurs in diabetic patients even before the diagnosis of diabetic retinopathy. Furthermore, thinning of both the nerve fiber and the RGC layer has been documented in patients with diabetic retinopathy (Verma et al., 2009; Vujosevic and Midena, 2013; Verbraak, 2014) and animal diabetic models (Oleg S. Gorbatyuk, 2021; Pitale et al., 2021). One of the earliest experimental observations in animal models of diabetic retinopathy (DR) was the impairment of retrograde axonal transport in RGCs (Potilinski et al., 2020). Interestingly, this impairment was found to be even greater in type 1 diabetes than in type 2 diabetes, possibly due to metabolic dysfunctions contributing to optic nerve atrophy (Zhang et al., 1998). Under high glucose conditions, there was an observed increase in glutamate release, leading to significant extracellular glutamate accumulation and subsequent neurotoxicity of RGCs, further contributing to their deterioration(Ma et al., 2010).

Various approaches have been employed to analyze cellular signaling involved in RGC death and axonal deterioration. For instance, research groups have conducted unbiased proteomic screens of total mouse retina lysates (Magharious et al., 2011; Hollander et al., 2012; Kwong et al., 2021; Zhu et al., 2022) and used fluorescent-assisted cell sorting (FACS)(Belin et al., 2015) to isolate RGCs following optic nerve crush (ONC), one of the most extensively studied models of CNS axonal injury. However, most of these studies either examined whole retina lysates or assessed sorted RGCs at a time point (3 days after injury) when a significant amount of RGC apoptosis has already began (Goldenberg-Cohen et al., 2012). Another common injury model is N-methyl-D-aspartate (NMDA)-induced excitotoxicity, a model mimicking the glutamate-induced excitotoxicity associated with multiple neurodegenerative diseases such as amyotrophic lateral sclerosis (ALS), ischemic stroke, and traumatic brain injury (Guerriero et al., 2015; Ibanez et al., 2022; Rubino et al., 2023). To date, the only study examining proteomics in the context of NMDA-induced excitotoxicity of RGCs investigated proteomic changes in whole retinal lysates 12 hours after NMDA injection, which is a time point at which a substantial amount of RGC apoptosis is already in progress (Suo et al., 2022).

Understanding how CNS neurons respond to injury is crucial as we strive to develop therapeutic strategies for promoting neuroprotection, axon survival, and regeneration. Particularly, the significance of such studies lies in the development of neuroprotective interventions. Therefore, we initiated a comparative proteomic study, in which we analyzed the protein profiles of RGCs subjected to different cellular stress stimuli. The importance of our study lies in the fact that we not only identified differentially expressed proteins involved in two distinct cell death mechanisms but also revealed common biological processes that were similarly altered by different cell stress stimuli.

2 Results

2.1 Nontargeted quantitative proteomics of retinal ganglion cells.

In our study, we adopted an approach to analyze molecular alterations in deteriorating RGCs before their cell death, even though the peaks of apoptosis occur at different time points. To investigate early proteomic changes in RGCs following ONC- or NMDA-induced injury, protein lysates from Thy1-magnetic bead-isolated RGCs underwent nano high-performance liquid chromatography/mass spectrometry (LC/MS). RGC enrichment was confirmed via western blot (WB) using antibodies against RGC proteins, RNA-binding protein with multiple splicing (Rbpms), Class III β-tubulin (Tubb3/TUJ1), and photoreceptor markers, phosphodiesterase 6β (Pde6β) and rhodopsin (Rho) (**Fig. 1A**). As expected, RGC markers Rbpms and Tubb3/TUJ1 were highly enriched in RGCs and notably reduced in cells not bound by Cd90.2-coupled magnetic beads, corresponding to the rest of the retinal cells (**Fig. 1A**). Furthermore, photoreceptor proteins Pde6β and rhodopsin were nearly undetectable in cells

bound by the beads but highly expressed in unbound retinal cells. RGC enrichment was further validated by quantitative reverse transcriptase polymerase chain reaction (qRT-PCR) with primers against CD90/Thy1, Rho, and Pde6b (**Fig. 1B**). While Thy1 was significantly elevated in cells bound by the magnetic beads and reduced in unbound cells, *Rho* and *Pde6b* mRNA levels were high in unbound cells and significantly diminished in bound cells. Together, the WB and qRT-PCR results indicate reliable RGC enrichment was achieved in our study.

We analyzed identified proteins and prior to pathway analysis, grouped them according to the following parameters: 1) elevated in NMDA treated 2) reduced in NMDA treated 3) elevated in ONC treated 4) reduced in ONC 5) altered in NMDA and ONC.

2.2 NMDA Treatment shifts RGC metabolic signaling.

To induce excitotoxic damage to the retina, we intravitreally injected 1 µl of 20 mM NMDA in PBS, following a protocol previously described (Guo et al., 2021). NMDA treatment resulted in significant alterations in multiple pathways, with a notable impact on metabolic processes (**Fig. 2** and **Table 1**). NMDA treatment induced a substantial increase in methylglyoxal (MGO) signaling and the pentose-phosphate pathway (PPP), indicating the involvement of oxidative stress and a decrease in glutathione (GSH) levels, which is often associated with increased apoptosis (Nuamnaichati et al., 2020; Barisa et al., 2021) (**Fig. 2A**). Consistent with these findings, the levels of specific proteins related to these pathways, such as GLO1 (Lactoylglutathione lyase, Q9CPU0) in the MGO signaling pathway and 6-phosphogluconolactonase (Q9CQ60) in the PPP, were significantly elevated (**Table 1**). Additionally, NMDA treatment led to an increase in NADPH regeneration, a process known to be derived from Glucose 6-phosphate (G6P). This regeneration involves enzymes such as G6P dehydrogenase, which generates NADPH, and 6-phosphogluconolactonase (Q9CQ60), which converts 6-phosphogluconolactone to 6-phosphogluconate. The elevated presence of 6-phosphogluconolactonase (Q9CQ60) in NMDA-treated RGCs was observed (Table 1). Furthermore, our study revealed an enhancement in protein sumoylation in NMDA-treated RGCs. This posttranslational modification plays a pivotal role in various biological functions, including nuclear-cytosolic transport, transcriptional regulation, apoptosis, and protein stability, among others.

Therefore, these findings demonstrate that NMDA treatment has a significant impact on metabolic signaling pathways in retinal ganglion cells, suggesting a link to oxidative stress, altered GSH levels, and increased apoptosis. Moreover, the study highlights the involvement of NADPH regeneration and protein sumoylation as part of the cellular responses to NMDA-induced excitotoxicity.

We then plotted proteins diminished following NMDA injections using the ShinyGo program. Fig. 2B and Table 1 clearly demonstrate that NMDA treatment results in a reduction of proteins associated with critical cellular processes, including the tricarboxylic acid (TCA) cycle, mitochondrial ATP-coupled

electron transport, aerobic respiration, and the respiratory electron transport chain. This reduction is particularly noteworthy as it predominantly affects mitochondrial proteins involved in essential functions (Table 1), ultimately leading to a decrease in adenosine triphosphate (ATP) production. Notably, NMDA excitotoxicity predominantly affects proteins crucial for ATP generation, underscoring its impact on cellular energy metabolism. Furthermore, our study identified specific cellular components that were enriched as a result of NMDA treatment. This enrichment notably included the mitochondrial respiratory chain complex III (involved in oxidative phosphorylation) and the oxidoreductase complex (specifically complex I: NADH-ubiquinone oxidoreductase). This elevation in these components aligns with the observed increase in various metabolic cellular processes (as depicted in Fig. 2C).

Collectively, our findings indicate that NMDA excitotoxicity in retinal ganglion cells leads to rapid perturbations in metabolic processes. These perturbations are characterized by a reduction in ATP production pathways and a simultaneous shift of glycolysis towards the PPP. This shift reflects the intricate interplay between NMDA-induced damage and cellular metabolic responses, shedding light on the complex mechanisms involved in excitotoxicity-induced cellular alterations.

2.3 ONC Results in an Early Shift in DNA Repair and Telomere Maintenance in RGCs.

RGCs were isolated 24 hours after the ONC procedure and subjected to LC/MS analysis. Examples of biological processes elevated following ONC include nucleosome organization, formation of protein-DNA complexes, DNA chromatin changes, and chromatin organization (**Fig. 3A**). These biological processes were accompanied by an increase in chromodomain-helicase-DNA-binding protein 4 (Q6PDQ2), histone H2B type 3-A (Q9D2U9), Histone H2B type 1-H (Q64478), and other nuclear proteins (**Table 2**). Among the reduced biological processes following ONC, we found that positive regulation of telomer and telomerase and spindle localization includes organelle localization (**Fig. 3B** and **Table 2**).

The GO Cellular component analysis demonstrates that an increase in proteins in ONC-processed RGCs was associated with endosome complex formation and CST, a cellular multiprotein complex involved in telomere maintenance (**Fig. 3C**). Therefore, it is not surprising that the endosomal Ras-related protein Rab-18 (P352930) was elevated. Other examples are the CST complex subunit STN1 (Q8K2X3) and High Mobility Group protein B3 (O54879) regulating the mechanisms of DNA replication, transcription, recombination, and repair that were significantly elevated in the ONC-processed RGCs (**Table 2**). We then found that reduced proteins were responsible for the GO cellular components, including the 6-phosphofructokinase complex and chaperon-containing T complex (CCT) (**Fig. 3D**). These findings were in accordance with the expression levels of individual proteins such as ATP-dependent 6-phosphofructokinases (P12382 and P47857) and T-complex protein 1 subunit

138 gamma (TRiC or P80318). Overall, these data suggested that ONC causes chromatin and DNA
139 reorganization in RGCs and reduces the cellular ability to repair DNA damage.
140
141 *2.4 Proteins altered following both NMDA-induced excitotoxicity and ONC.*
142 One of the primary objectives of this study was to identify proteins that exhibit changes in multiple
143 models of neuronal injury. In pursuit of this goal, we successfully identified proteins that exhibited
144 alterations in both models (**Fig. 4** and **Table 3**). Remarkably, the majority of these protein level changes,
145 whether upregulation or downregulation, were notably consistent across both groups. Specifically, we
146 observed significant upregulation of eukaryotic initiation factor 4A-II (4A-II), small nuclear
147 ribonucleoprotein D3 (SNRD3), and STN1, alongside significant downregulation of Ras-related protein
148 (Rab-18), AP-1, Clathrin, ATP synthase subunit D, and sodium and chloride-dependent GABA
149 transporter 3 in both treated RGCs when compared to the control group. Fig. 4, which provides a visual
150 representation of these modified protein levels, also highlights the unique absence of succinate
151 semialdehyde dehydrogenase (SSADH) and KCNB2 (potassium voltage-gated channel subfamily B
152 member 2) in both RGC treatments as compared to control.
153 The analysis of differentially expressed proteins revealed 16 proteins with significantly reduced
154 expression, four proteins with significantly increased expression, one protein exhibiting an opposite
155 response pattern to the stimulus in both types of treated RGCs, and two proteins uniquely present in
156 the control group.
157
158 **3 Discussion**
159 In the present study, we examined acute changes in RGC global protein expression following
160 NMDA injection or ONC. We provide evidence that NMDA treatment alters multiple signaling pathways,
161 many of which are metabolic. In addition, we identified several biological processes impacted by ONC.
162 We identified common proteins manifesting a decline and incline in expression and unique proteins
163 absent in RGC undergoing both types of injury.
164 Classically, the primary cause of glutamate excitotoxicity is ATP depletion and impaired
165 glutamate transport, resulting in a buildup of extracellular glutamate, leading to excitotoxicity by
166 overloading NMDA receptor (NMDAR)-expressing cells with Na+ and Ca2+. Glutamate excitotoxicity is
167 known to be involved in various diseases, including Alzheimer's (Tannenberg et al., 2004), Parkinson's
168 (Verma et al., 2022), or Huntington's (Girling et al., 2018), and predicted to be involved in choroidal
169 vessel occlusion, glaucoma, and diabetic retinopathy (Lucas and Newhouse, 1957; Massey and Miller,
170 1987, 1990; Thoreson and Witkovsky, 1999; Yumnamcha et al., 2020). Elevated Ca2+ can lead to
171 changes in several Ca2+-sensitive signaling cascades and eventually mitochondrial-mediated
172 apoptosis (Verma et al., 2022). An increase in intracellular Na+ can lead to cell swelling. NMDA-

173 mediated excitotoxicity leads to synaptic degeneration and dendritic pruning before cell death. By
174 isolating RGCs one hour after NMDA injection, we hoped to see how the RGCs are altered in the time
175 window before full-fledged apoptosis begins. We did indeed observe perturbations in several biological
176 processes after NMDA injection. We report that early NMDA-induced excitotoxicity leads to a
177 substantial elevation of MGO and the PPP, indicating a potential involvement of oxidative stress and a
178 reduction in the levels of GSH, which is often associated with apoptosis. Despite this, we did not
179 observe a significant change in GO biological processes pertaining to apoptosis or any other known
180 form of cell death, indicating we did indeed perform proteomic analysis at a time point after NMDA-
181 induced excitotoxicity where apoptotic signaling is not yet elevated. In addition, we also discovered that
182 many of the cellular processes upregulated by excitotoxicity involve changes in the nucleus, such as
183 nuclear protein export, and regulation of DNA processes (**Fig. 2A**). These specific changes could
184 represent heterogeneous nuclear ribonucleoprotein A1, A1/B1, small nuclear ribonucleoprotein D3.

185 We also show that NMDA treatment reduces many GO biological processes. Of note, most
186 proteins reduced by intravitreal NMDA injection are involved in ATP production. It is possible that the
187 calcium elevation that occurs during excitotoxicity could be the major driving force behind excitotoxic
188 cell death. Cells respond to this is by sequestering this excess calcium in the endoplasmic reticulum
189 and mitochondria. Mitochondria is the site of oxidative phosphorylation, a process that generates ATP
190 and is regulated by calcium (Glancy et al., 2013). This is consistent with our findings on a reduction of
191 GO biological processes pertaining to ATP production and a decline in GO cellular components
192 pertaining to various mitochondrial complexes.

193 The murine optic nerve crush injury model is the most commonly used model of RGC injury that
194 mimics molecular events occurring upon traumatic optic neuropathy, glaucoma, etc. (Tang et al., 2011)
195 Moreover, the prevalence of optic neuropathy in diabetics could increase with diabetes duration (Hua
196 et al., 2019) In this model, the crush injury to the optic nerve leads to retinal ganglion cell apoptosis.
197 This disease model can be used to study the general processes and mechanisms of neuronal death
198 and survival, which is essential for the development of therapeutic measures. In addition,
199 pharmacological and molecular approaches can be used in this model to identify and test potential
200 therapeutic reagents to treat different types of optic neuropathy. Interventions that are neuroprotective
201 for RGCs challenged with ONC are usually neuroprotective for other CNS neurons (Le Pichon et al.,
202 2017). In addition, axon regeneration promoting treatments discovered with the ONC model can
203 typically promote axon regeneration in the spinal cord (Bhowmick and Abdul-Muneer, 2021). Following
204 ONC, axonal components briefly travel retrogradely prior to the axons returning to the site of injury,
205 only to fail to pass the crush site. In fact, knocking out an inhibitor of the retrograde injury response of
206 RGCs, dual-leucine zipper kinase (DLK), leads to robust RGC survival (Watkins et al., 2013), indicating
207 that retrograde signaling is crucial for cell death signaling following ONC. Based on this, in the earliest

response to ONC, we would anticipate changes in the machinery responsible for transport and localization. As expected, we did identify reductions in GO biological processes pertaining to the localization of organelles cellular proteins and cellular macromolecules. After injuring the axon with ONC, we expected to observe changes in synaptic GO cellular components. To that end, we did detected changes in components of synaptic membrane, synapse, neuronal projections, the presynapse, and the presynaptic membrane region. These changes are presented by the decline in multiple proteins including Catenin beta-1, Sodium- and chloride-dependent GABA transporter 3, Synaptogyrin-3 and Synaptotagmin-1. Together, these changes in GO biological processes and cellular components after ONC suggest that, as expected, damaging the axon not only disrupts axonal components but also the cellular localization of various cellular entities.

In both RGC degenerative models, we identified common proteins that responded to cellular insults in a similar manner, as well as proteins that exhibited a unique decline in expression in both challenged RGCs. While our current study has its limitations, future investigations should prioritize the validation of the roles of these proteins in RGC survival. In particular, it would be interesting to assess the role of these proteins in RGC survival during the development of diabetic retinopathy or glaucoma. For example, Rab18 deficiency detected in both types of challenged RGCs is the molecular deficit underlying Warburg micro syndrome, characterized by eye, nervous system, and endocrine abnormalities.(Handley and Sheridan, 1993) Moreover, a recent study highlighted the involvement of Rab18 in lipid metabolism in human diabetic adipose tissue and demonstrated that Rab-18 contributes to insulin resistance in obese individuals. (Pulido et al., 2011; Guzman-Ruiz et al., 2020) Another example is DnaJC8 protein, the effect of which is closely associated with the aggregation of polyQ-containing proteins in a cellular model of spinocerebellar ataxia type 3 (SCA3).(Ito et al., 2016) The authors have shown that DnaJC8 overexpression significantly reduces polyQ aggregation and apoptosis. Therefore, DnaJC8 should be validated for its neuroprotective role in the survival of RGCs undergoing both cellular stressors. Finally, both KCNB2 and SSADH are exclusively present in control C57BL6 RGCs and are absent in both types of challenged RGCs. Similar to SSADH deficiency representing a genetic disorder resulting from the aberrant metabolism of GABA (Didiasova et al., 2020), loss of SSDAH could be a consequence of a defective GABA catabolism in both types of stressed RGCs.

In summary, our study was designed to not only identify both individual and shared proteomic changes in retinal ganglion cells undergoing different stress stimuli just before initiating a pro-apoptotic cell death program but also to lay the groundwork for the future development of a therapeutic platform for testing gene candidates contributing to retinal diseases such as diabetic retinopathy and glaucoma.

4 Conclusion

243 Here we report that challenging RGCs alters the levels of various proteins and therefore likely
244 impact cellular signaling at the onset of damage. We utilized unbiased, non-targeted proteomics to
245 identify proteins and GO biological processes altered after ONC or NMDA-induced excitoxicity. NMDA-
246 induced excitoxicity resulted in altered metabolic signaling. We observed a noticeable reduction in
247 proteins and GO biological processes involved in ATP production. NMDA led to an increase in MGO
248 signaling and the PPP, indicating the involvement of oxidative stress and a decrease in GSH levels.
249 RGCs experienced a shift in DNA repair and telomere maintenance 24 hours after ONC. Further
250 characterization of these altered proteins and signaling pathways may be vital for the creation of
251 therapeutic countermeasures for neurodegenerative diseases.
252

253 **5 Methods**

254 *5.1 Animals*

255 All animal procedures were approved by The University of Alabama at Birmingham institutional
256 animal use and care (IACUC) committee and in accordance with the statement for the Use of Animals
257 in Ophthalmic and Vision Research by The Association for Research in Vision and Ophthalmology
258 (ARVO). C57BL/6J mice were purchased from Jackson Laboratory (Bar Harbor, ME). An equal number
259 of female and male mice were used in this study. For all procedures, mice were anesthetized with
260 ketamine (100 mg/kg) and xylazine (10mg/kg).

261 To induce injury to RGCs, mice were either intravitreally injected with 1µl of 20mM N-Methyl D
262 aspartic acid (NMDA) or underwent optic nerve crush (ONC) surgery as previously described (Guo et
263 al., 2021). Briefly, for ONC, fine tweezers (Dumont#5; Fine Science Tools (FST) Item No. 11254-20 or
264 Dumont#55; FST Item No. 11255-20) were used to create a small incision in the conjunctiva and then
265 maneuvered between extraocular muscles to access the optic nerve, which was gently squeezed for 5
266 seconds at a location approximately 1mm posterior to the globe using Dumont #5 tweezers.
267

268 *5.2 RGC Isolation*

269 To isolate RGCs, we used a method that has previously been verified with slight modifications.
270 Briefly, animals from each group were euthanized with CO_2 asphyxiation and their retinas were
271 harvested in cold neurobasal medium and placed in a 37°C water bath for 5 minutes. The neurobasal
272 media was removed and replaced with fresh pre-warmed neurobasal media containing papain
273 (0.06mg/ml or 33.4 U/mg) and 5mM L-cysteine and incubated 20 minutes at 37°C. The papain solution
274 was removed and replaced with neurobasal containing 2mM L-Glutamine (Gibco; Catalog no.
275 25030081) B-27 supplement (Gibco; Catalog no. 17504044) and 10% FBS (Gibco; Catalog no.
276 26140079). The retinas were dissociated by gently pipetting up and down with a wide bore 1ml pipette
277 tip. Cells were then centrifuged at 450g for 8 minutes and resuspended in 90 µl of isolation buffer

278 (DPBS + 0.5% BSA + 2mM EDTA) containing 25 µg/ml DNAse I + 5mM MgCl2. Cells were filtered
279 through a 30µm cell strainer and incubated with CD90.2 magnetic beads (Miltenyi Biotec; Catalog no.
280 130-121-278) at 4°C for 10 minutes and then isolated using MACs LS (Miltenyi Biotec; Catalog no. 130-
281 042-401) columns following the manufacturer's instructions. After isolation, cells were washed with
282 DPBS, centrifuged at 450g for 8 minutes and their pellets stored at -70°C prior to proteomics sample
283 preparation and LC/MS analysis.
284
285 *5.3 Proteomics*
286 *5.3.1 LC/MS*
287 Proteomics analysis was carried out as previously described with minor changes (Ludwig et al.,
288 2016), within section 2.5 nLC-ESI-MS2 under Protein IDs for GeLC. Proteins from isolated RGCs were
289 extracted using T-PER™ Mammalian Protein Extraction Reagent (Thermo Fisher Scientific, Cat.#
290 78510) supplemented with HALT protease inhibitor cocktail (Thermo Fisher Scientific, Cat.# 78425),
291 and benzonase nuclease (Sigma, E1014) following manufacturers instructions. Lysates were quantified
292 using Pierce BCA Protein Assay Kit (Thermo Fisher Scientific, Cat.# 23227). Samples were prepared
293 in NuPAGE LDS sample buffer (1x final conc., Invitrogen, Cat.# NP0007) and reduced with DTT then
294 denatured at 70°C for 10min prior to loading 20µg onto Novex NuPAGE 10% Bis-Tris Protein gels
295 (Invitrogen, Cat.# NP0315BOX) and separated appropriately (@ 200 constant V). The gels were
296 stained overnight with Novex Colloidal Blue Staining kit (Invitrogen, Cat.# LC6025). Following de-
297 staining, each entire lane was cut into multiple MW and equilibrated in 100 mM ammonium bicarbonate
298 (AmBc), each gel plug was then digested overnight with Trypsin Gold, Mass Spectrometry Grade
299 (Promega, Cat.# V5280) following manufacturer's instruction. Peptide extracts were reconstituted in
300 0.1% Formic Acid/ddH2O at 0.1µg/µL.
301 Peptide digests (8µL each) were injected onto a 1260 Infinity nHPLC stack (Agilent
302 Technologies), and separated using a 75 micron I.D. x 15 cm pulled tip C-18 column (Jupiter C-18 300
303 Å, 5 micron, Phenomenex). This system runs in-line with a Thermo Q Exactive HFx mass spectrometer,
304 equipped with a Nanospray Flex™ ion source (Thermo Fisher Scientific), and all data were collected in
305 CID mode. The nHPLC is configured with binary mobile phases that includes solvent A (0.1%FA in
306 ddH2O), and solvent B (0.1%FA in 15% ddH2O/85% ACN), programmed as follows; 10min @ 5%B
307 (2µL/min, load), 30min @ 5%-40%B (linear: 0.5nL/min, analyze), 5min @ 70%B (2µL/min, wash),
308 10min @ 0%B (2µL/min, equilibrate). Following each parent ion scan (300-1200m/z @ 60k resolution),
309 fragmentation data (MS2) were collected on the top most intense 18 ions @7.5K resolution. For data
310 dependent scans, charge state screening and dynamic exclusion were enabled with a repeat count of
311 2, repeat duration of 30s, and exclusion duration of 90s.

312 MS data conversion and searches The XCalibur RAW files were collected in profile mode,
313 centroided and converted to MzXML using ReAdW v. 3.5.1. The mgf files were created using
314 MzXML2Search (included in TPP v. 3.5) for all scans. The data was searched using SEQUEST
315 (Thermo Fisher Scientific), which is set for three maximum missed cleavages, a precursor mass window
316 of 20ppm, trypsin digestion, variable modification C @ 57.0293, and M @ 15.9949 as a base setting.
317 Searches were performed with the mus musculus species specific subset of the UniProtKB database.
318

319 *5.3.2 Peptide filtering, grouping, and quantification*

320 The list of peptide IDs generated based on SEQUEST search results were filtered using Scaffold
321 (Protein Sciences, Portland Oregon). Scaffold filters and groups all peptides to generate and retain only
322 high confidence IDs while also generating normalized spectral counts (N-SC's) across all samples for
323 the purpose of relative quantification. The filter cut-off values were set with minimum peptide length of
324 >5 AA's, with no MH+1 charge states, with peptide probabilities of >80% C.I., and with the number of
325 peptides per protein ≥2. The protein probabilities will be set to a >99.0% C.I., and an FDR<1.0. Scaffold
326 incorporates the two most common methods for statistical validation of large proteome datasets, the
327 false discovery rate (FDR) and protein probability (Keller, Nesvizhskii, Weatherly). Relative
328 quantification across experiments were then performed via spectral counting (Old, Liu), and when
329 relevant, spectral count abundances will then be normalized between samples (Hyde).
330

331 *5.3.3 Statistical analysis*

332 For generated proteomic data, two separate non-parametric-like statistical analyses were
333 performed between each pair-wise comparison. These analyses included; A) the calculation of weight
334 values by significance analysis of microarray (SAM; cut off >|0.8| combined with, B) T-Test (single tail,
335 unequal variance, cut off of $p < 0.05$), which are then sorted according to the highest statistical
336 relevance in each comparison. For SAM, the weight value (W) is a function statistically derived that
337 approaches significance as the distance between the means ($\mu1-\mu2$) for each group increases, and the
338 SD ($\delta1-\delta2$) decreases using the formula: $W=(\mu1-\mu2)/(\delta1-\delta2)$. For protein abundance ratios determined
339 with N-SC's, we set a 1.5-fold change as the threshold for significance, determined empirically by
340 analyzing the inner-quartile data from the control experiments using ln-ln plots, where the Pierson's
341 correlation coefficient (R) is 0.98, and >99% of the normalized intensities fell between the set fold
342 change. Each of the tests (SAM, Ttest, and fold change) must be passed for to be considered
343 significant.
344

345 *5.3.4 Systems Analysis*

346 Gene ontology assignments and pathway analysis were carried out using ShinyGO (Ge et al., 2020).

6 Funding

This work was supported by the National Eye Institute, grants R01 EY027763.

7 Conflict of Interests statement

The authors declare that the research was conducted in the absence of any commercial or financial relationships that could be construed as a potential conflict of interest.

372 **Figure Legends**

373 **Figure 1**- RGCs are enriched with Cd90.2 coupled magnetic beads. A) Western blot of select RGC and
374 photoreceptor proteins indicating RGC enrichment. B) qRT-PCR analysis using primers against RGC
375 or photoreceptor targets. * = $p<0.05$, *** = $p<0.005$, **** = $p<0.001$ (n=3-4). Data are shown as a
376 standard deviation.

377 **Figure 2**- GO biological processes and cellular components of RGCs shift 1 hour after intravitreal
378 NMDA injection. A) The most significantly elevated GO biological processes following NMDA-induced
379 excitoxicity. B) GO biological processes reduced by intravitreal NMDA injection. C) GO cellular
380 components reduced by NMDA-induced excitoxicity. False Discovery rate (FDR) ≥ 0.05.

381 **Figure 3** - GO biological processes and cellular components of RGCs shift 24 hours after ONC. A) The
382 most significantly elevated GO biological processes following traumatic injury to the optic nerve. B) GO
383 biological processes reduced by ONC. C) GO cellular components elevated by ONC. D) GO cellular
384 components reduced 24 hours after ONC. False Discovery rate (FDR) ≥ 0.05.

385 **Figure 4** – Select proteins with signficantly altered levels after both NMDA injection and ONC. Levels
386 depicted have been normalized to control. All proteins that are changed in both models of RGC injury
387 are listed in table 3 (n=4). Data are shown as a standard error.

388 **Table Legends**

389 **Table 1**- List of proteins differentially expressed in RGCs 1 hour after NMDA treatment. The accession
390 numbers were entered into ShinyGO to generate Figure 2.
391
392 **Table 2-** List of proteins differentially expressed in RGCs 24 hours after ONC. Accesion numbers were
393 entered into ShinyGO to generate Figure 3.
394
395 **Table 3-** List of proteins altered after both NMDA injection and after ONC.
396
397
398
399
400
401
402
403
404
405
406
407
408
409

References

Abu-El-Asrar AM, Dralands L, Missotten L, Al-Jadaan IA, Geboes K (2004) Expression of apoptosis markers in the retinas of human subjects with diabetes. Invest Ophthalmol Vis Sci 45:2760-2766.

Barisa M, Fowler D, Fisher J (2021) Interplay between gammadeltaT-Cell Metabolism and Tumour Microenvironment Offers Opportunities for Therapeutic Intervention. Immunometabolism 3:210026.

Belin S, Nawabi H, Wang C, Tang S, Latremoliere A, Warren P, Schorle H, Uncu C, Woolf CJ, He Z, Steen JA (2015) Injury-Induced Decline of Intrinsic Regenerative Ability Revealed by Quantitative Proteomics. Neuron 86:1000-1014.

Bhowmick S, Abdul-Muneer PM (2021) PTEN Blocking Stimulates Corticospinal and Raphespinal Axonal Regeneration and Promotes Functional Recovery After Spinal Cord Injury. J Neuropathol Exp Neurol 80:169-181.

Bikbova G, Oshitari T, Baba T, Yamamoto S (2014) Neurotrophic factors for retinal ganglion cell neuropathy - with a special reference to diabetic neuropathy in the retina. Curr Diabetes Rev 10:166-176.

Didiasova M, Banning A, Brennenstuhl H, Jung-Klawitter S, Cinquemani C, Opladen T, Tikkanen R (2020) Succinic Semialdehyde Dehydrogenase Deficiency: An Update. Cells 9.

Ge SX, Jung D, Yao R (2020) ShinyGO: a graphical gene-set enrichment tool for animals and plants. Bioinformatics 36:2628-2629.

Girling KD, Demers MJ, Laine J, Zhang S, Wang YT, Graham RK (2018) Activation of caspase-6 and cleavage of caspase-6 substrates is an early event in NMDA receptor-mediated excitotoxicity. J Neurosci Res 96:391-406.

Glancy B, Willis WT, Chess DJ, Balaban RS (2013) Effect of calcium on the oxidative phosphorylation cascade in skeletal muscle mitochondria. Biochemistry 52:2793-2809.

Goldenberg-Cohen N, Raiter A, Gaydar V, Dratviman-Storobinsky O, Goldstein T, Weizman A, Hardy B (2012) Peptide-binding GRP78 protects neurons from hypoxia-induced apoptosis. Apoptosis 17:278-288.

Guerriero RM, Giza CC, Rotenberg A (2015) Glutamate and GABA imbalance following traumatic brain injury. Curr Neurol Neurosci Rep 15:27.

Guo X, Starr C, Zhou J, Chen B (2021) Protocol for evaluating the role of a gene in protecting mouse retinal ganglion cells. STAR Protoc 2:100932.

Guzman-Ruiz R, Tercero-Alcazar C, Rabanal-Ruiz Y, Diaz-Ruiz A, El Bekay R, Rangel-Zuniga OA, Navarro-Ruiz MC, Molero L, Membrives A, Ruiz-Rabelo JF, Pandit A, Lopez-Miranda J, Tinahones FJ, Malagon MM (2020) Adipose tissue depot-specific intracellular and extracellular cues contributing to insulin resistance in obese individuals. FASEB J 34:7520-7539.

Handley M, Sheridan E (1993) RAB18 Deficiency. In: GeneReviews((R)) (Adam MP, Mirzaa GM, Pagon RA, Wallace SE, Bean LJH, Gripp KW, Amemiya A, eds). Seattle (WA).

Hollander A, D'Onofrio PM, Magharious MM, Lysko MD, Koeberle PD (2012) Quantitative retinal protein analysis after optic nerve transection reveals a neuroprotective role for hepatoma-derived growth factor on injured retinal ganglion cells. Invest Ophthalmol Vis Sci 53:3973-3989.

Hua R, Qu L, Ma B, Yang P, Sun H, Liu L (2019) Diabetic Optic Neuropathy and Its Risk Factors in Chinese Patients With Diabetic Retinopathy. Invest Ophthalmol Vis Sci 60:3514-3519.

Ibanez L et al. (2022) Multi-ancestry GWAS reveals excitotoxicity associated with outcome after ischaemic stroke. Brain 145:2394-2406.

Ito N, Kamiguchi K, Nakanishi K, Sokolovskya A, Hirohashi Y, Tamura Y, Murai A, Yamamoto E, Kanaseki T, Tsukahara T, Kochin V, Chiba S, Shimohama S, Sato N, Torigoe T (2016) A novel nuclear DnaJ protein, DNAJC8, can suppress the formation of spinocerebellar ataxia 3 polyglutamine aggregation in a J-domain independent manner. Biochem Biophys Res Commun 474:626-633.

461 Joo CK, Choi JS, Ko HW, Park KY, Sohn S, Chun MH, Oh YJ, Gwag BJ (1999) Necrosis and
462 apoptosis after retinal ischemia: involvement of NMDA-mediated excitotoxicity and p53. Invest
463 Ophthalmol Vis Sci 40:713-720.
464 Khan RS, Ross AG, Aravand P, Dine K, Selzer EB, Shindler KS (2021) RGC and Vision Loss From
465 Traumatic Optic Neuropathy Induced by Repetitive Closed Head Trauma Is Dependent on
466 Timing and Force of Impact. Transl Vis Sci Technol 10:8.
467 Kuehn MH, Fingert JH, Kwon YH (2005) Retinal ganglion cell death in glaucoma: mechanisms and
468 neuroprotective strategies. Ophthalmol Clin North Am 18:383-395, vi.
469 Kwong JMK, Caprioli J, Sze YH, Yu FJ, Li KK, To CH, Lam TC (2021) Differential Retinal Protein
470 Expression in Primary and Secondary Retinal Ganglion Cell Degeneration Identified by
471 Integrated SWATH and Target-Based Proteomics. Int J Mol Sci 22.
472 Le Pichon CE et al. (2017) Loss of dual leucine zipper kinase signaling is protective in animal models
473 of neurodegenerative disease. Science Translational Medicine 9:eaag0394.
474 Lucas DR, Newhouse JP (1957) The toxic effect of sodium L-glutamate on the inner layers of the
475 retina. AMA Arch Ophthalmol 58:193-201.
476 Ludwig MR, Kojima K, Bowersock GJ, Chen D, Jhala NC, Buchsbaum DJ, Grizzle WE, Klug CA,
477 Mobley JA (2016) Surveying the serologic proteome in a tissue-specific kras(G12D) knockin
478 mouse model of pancreatic cancer. Proteomics 16:516-531.
479 Ma R, Xie XJ, Wan L (2010) [Effect of drug-serum with Chinese drugs for nourishing shen and
480 activating blood on the glutamate release in purified retinal ganglion cells cultured in high-
481 glucose conditions]. Zhongguo Zhong Xi Yi Jie He Za Zhi 30:875-879.
482 Magharious M, D'Onofrio PM, Hollander A, Zhu P, Chen J, Koeberle PD (2011) Quantitative iTRAQ
483 analysis of retinal ganglion cell degeneration after optic nerve crush. J Proteome Res 10:3344-
484 3362.
485 Massey SC, Miller RF (1987) Excitatory amino acid receptors of rod- and cone-driven horizontal cells
486 in the rabbit retina. J Neurophysiol 57:645-659.
487 Massey SC, Miller RF (1990) N-methyl-D-aspartate receptors of ganglion cells in rabbit retina. J
488 Neurophysiol 63:16-30.
489 Nuamnaichati N, Mangmool S, Chattipakorn N, Parichatikanond W (2020) Stimulation of GLP-1
490 Receptor Inhibits Methylglyoxal-Induced Mitochondrial Dysfunctions in H9c2 Cardiomyoblasts:
491 Potential Role of Epac/PI3K/Akt Pathway. Front Pharmacol 11:805.
492 Oleg S. Gorbatyuk PMP, Irina V. Saltykova, Iuliia B. Dorofeeva, Assylbek A. Zhylkibayev, Mohammad
493 Athar, Preston A. Fuchs, Brian C. Samuels and Marina S. Gorbatyuk (2021) A Novel Tree
494 Shrew Model of Diabetic Retinopathy. Front Endocrinol (Lausanne).
495 Pitale PM, Saltykova IV, Adu-Agyeiwaah Y, Calzi SL, Satoh T, Akira S, Gorbatyuk O, Boulton ME,
496 Pardue MT, Garvey WT, Athar M, Grant MB, Gorbatyuk MS (2021) Tribbles Homolog 3
497 Mediates the Development and Progression of Diabetic Retinopathy. Diabetes.
498 Potilinski MC, Lorenc V, Perisset S, Gallo JE (2020) Mechanisms behind Retinal Ganglion Cell Loss
499 in Diabetes and Therapeutic Approach. Int J Mol Sci 21.
500 Pulido MR, Diaz-Ruiz A, Jimenez-Gomez Y, Garcia-Navarro S, Gracia-Navarro F, Tinahones F,
501 Lopez-Miranda J, Fruhbeck G, Vazquez-Martinez R, Malagon MM (2011) Rab18 dynamics in
502 adipocytes in relation to lipogenesis, lipolysis and obesity. PLoS One 6:e22931.
503 Rubino V, La Rosa G, Pipicelli L, Carriero F, Damiano S, Santillo M, Terrazzano G, Ruggiero G,
504 Mondola P (2023) Insights on the Multifaceted Roles of Wild-Type and Mutated Superoxide
505 Dismutase 1 in Amyotrophic Lateral Sclerosis Pathogenesis. Antioxidants (Basel) 12.
506 Shen WC, Huang BQ, Yang J (2023) Regulatory mechanisms of retinal ganglion cell death in normal
507 tension glaucoma and potential therapies. Neural Regen Res 18:87-93.
508 Sucher NJ, Lipton SA, Dreyer EB (1997) Molecular basis of glutamate toxicity in retinal ganglion cells.
509 Vision Res 37:3483-3493.
510 Suo L, Dai W, Chen X, Qin X, Li G, Song S, Zhang D, Zhang C (2022) Proteomics analysis of N-
511 methyl-d-aspartate-induced cell death in retinal and optic nerves. J Proteomics 252:104427.

512 Tang Z, Zhang S, Lee C, Kumar A, Arjunan P, Li Y, Zhang F, Li X (2011) An optic nerve crush injury
513 murine model to study retinal ganglion cell survival. J Vis Exp.
514 Tannenberg RK, Scott HL, Westphalen RI, Dodd PR (2004) The identification and characterization of
515 excitotoxic nerve-endings in Alzheimer disease. Curr Alzheimer Res 1:11-25.
516 Thoreson WB, Witkovsky P (1999) Glutamate receptors and circuits in the vertebrate retina. Prog
517 Retin Eye Res 18:765-810.
518 Verbraak FD (2014) Neuroretinal degeneration in relation to vasculopathy in diabetes. Diabetes
519 63:3590-3592.
520 Verma A, Rani PK, Raman R, Pal SS, Laxmi G, Gupta M, Sahu C, Vaitheeswaran K, Sharma T
521 (2009) Is neuronal dysfunction an early sign of diabetic retinopathy? Microperimetry and
522 spectral domain optical coherence tomography (SD-OCT) study in individuals with diabetes,
523 but no diabetic retinopathy. Eye (Lond) 23:1824-1830.
524 Verma M, Lizama BN, Chu CT (2022) Excitotoxicity, calcium and mitochondria: a triad in synaptic
525 neurodegeneration. Transl Neurodegener 11:3.
526 Vujosevic S, Midena E (2013) Retinal layers changes in human preclinical and early clinical diabetic
527 retinopathy support early retinal neuronal and Muller cells alterations. J Diabetes Res
528 2013:905058.
529 Watkins TA, Wang B, Huntwork-Rodriguez S, Yang J, Jiang Z, Eastham-Anderson J, Modrusan Z,
530 Kaminker JS, Tessier-Lavigne M, Lewcock JW (2013) DLK initiates a transcriptional program
531 that couples apoptotic and regenerative responses to axonal injury. Proceedings of the
532 National Academy of Sciences 110:4039-4044.
533 Yumnamcha T, Guerra M, Singh LP, Ibrahim AS (2020) Metabolic Dysregulation and Neurovascular
534 Dysfunction in Diabetic Retinopathy. Antioxidants (Basel) 9.
535 Zhang L, Inoue M, Dong K, Yamamoto M (1998) Alterations in retrograde axonal transport in optic
536 nerve of type I and type II diabetic rats. Kobe J Med Sci 44:205-215.
537 Zhu Y, Zhang Y, Qi X, Lian Y, Che H, Jia J, Yang C, Xu Y, Chi X, Jiang W, Li Y, Mi J, Yang Y, Li X,
538 Tian G (2022) GAD1 alleviates injury-induced optic neurodegeneration by inhibiting retinal
539 ganglion cell apoptosis. Exp Eye Res 223:109201.

540

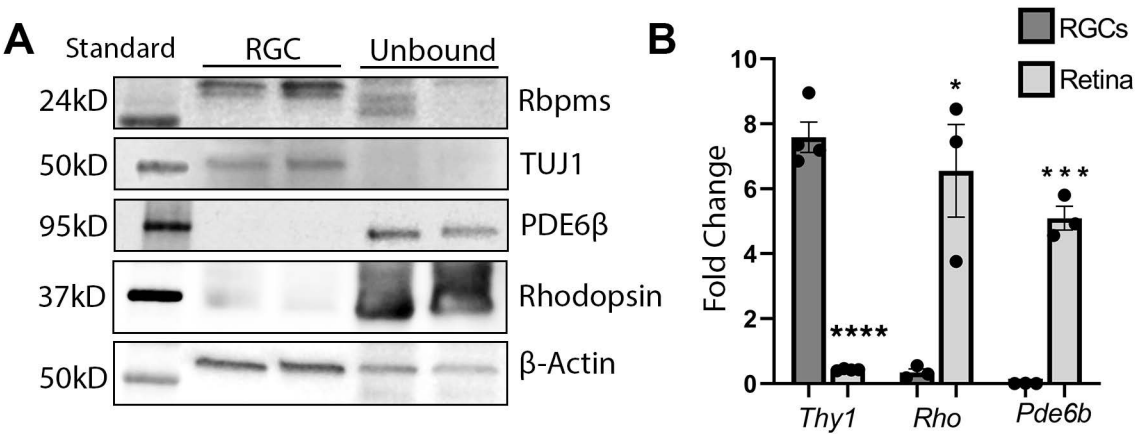
A
Standard
RGC
Unbound
24kD
Rbpms
50kD
TUJ1
95kD
PDE6β
37kD
Rhodopsin
50kD
β-Actin
B
RGCs
Retina
Fold Change
10
8
6
4
2
0
****
*
***
Thy1
Rho
Pde6b

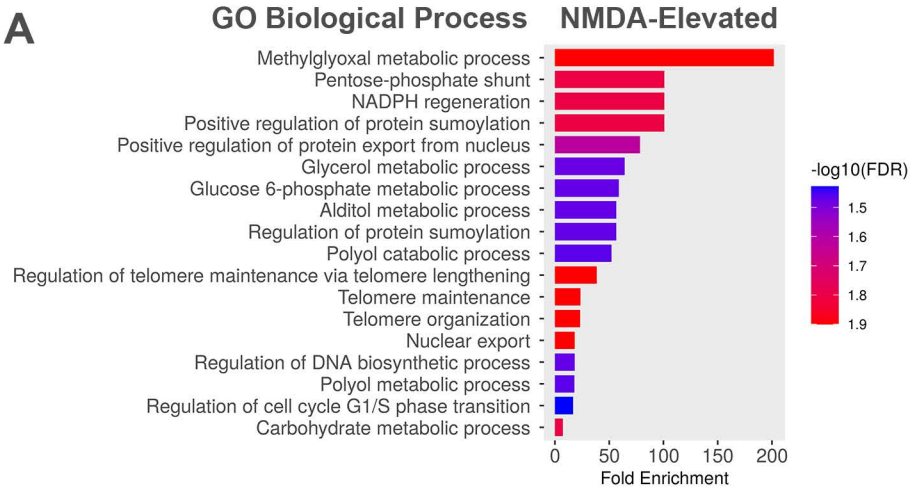
A
GO Biological Process
NMDA-Elevated
Methylglyoxal metabolic process
Pentose-phosphate shunt
NADPH regeneration
Positive regulation of protein sumoylation
Positive regulation of protein export from nucleus
Glycerol metabolic process
Glucose 6-phosphate metabolic process
Alditol metabolic process
Regulation of protein sumoylation
Polyol catabolic process
Regulation of telomere maintenance via telomere lengthening
Telomere maintenance
Telomere organization
Nuclear export
Regulation of DNA biosynthetic process
Polyol metabolic process
Regulation of cell cycle G1/S phase transition
Carbohydrate metabolic process
0
50
100
150
200
Fold Enrichment
-log10(FDR)
1.5
1.6
1.7
1.8
1.9

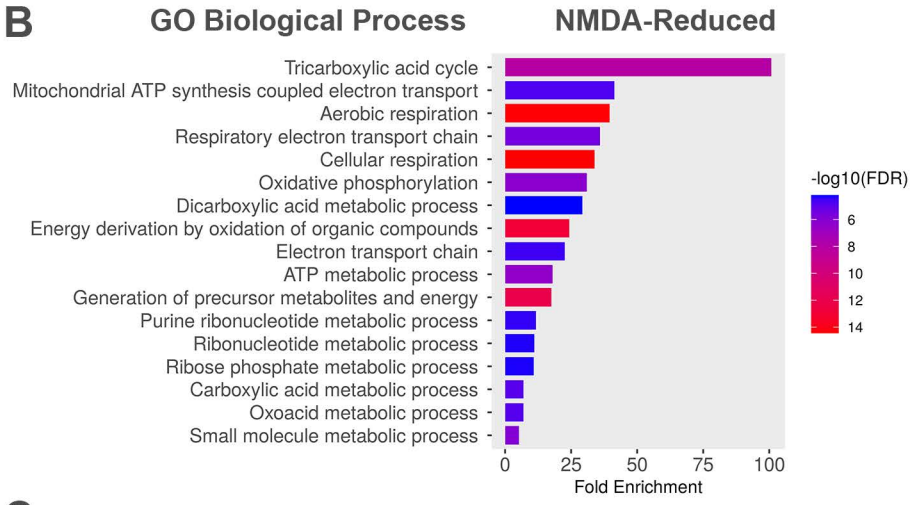
B
GO Biological Process
NMDA-Reduced
Tricarboxylic acid cycle
Mitochondrial ATP synthesis coupled electron transport
Aerobic respiration
Respiratory electron transport chain
Cellular respiration
Oxidative phosphorylation
Dicarboxylic acid metabolic process
Energy derivation by oxidation of organic compounds
Electron transport chain
ATP metabolic process
Generation of precursor metabolites and energy
Purine ribonucleotide metabolic process
Ribonucleotide metabolic process
Ribose phosphate metabolic process
Carboxylic acid metabolic process
Oxoacid metabolic process
Small molecule metabolic process
0
25
50
75
100
Fold Enrichment
-log10(FDR)
6
8
10
12
14

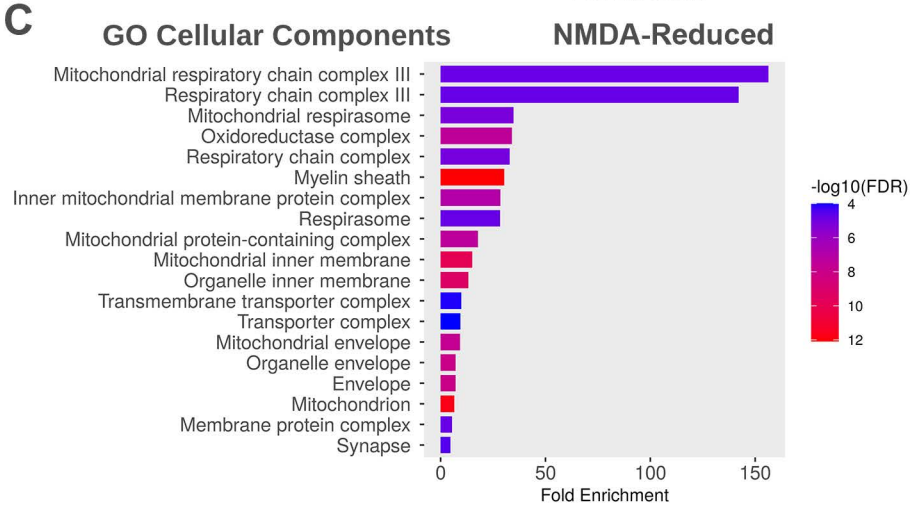
C
GO Cellular Components
NMDA-Reduced
Mitochondrial respiratory chain complex III
Respiratory chain complex III
Mitochondrial respirasome
Oxidoreductase complex
Respiratory chain complex
Myelin sheath
Inner mitochondrial membrane protein complex
Respirasome
Mitochondrial protein-containing complex
Mitochondrial inner membrane
Organelle inner membrane
Transmembrane transporter complex
Transporter complex
Mitochondrial envelope
Organelle envelope
Envelope
Mitochondrion
Membrane protein complex
Synapse
0
50
100
150
Fold Enrichment
-log10(FDR)
4
6
8
10
12

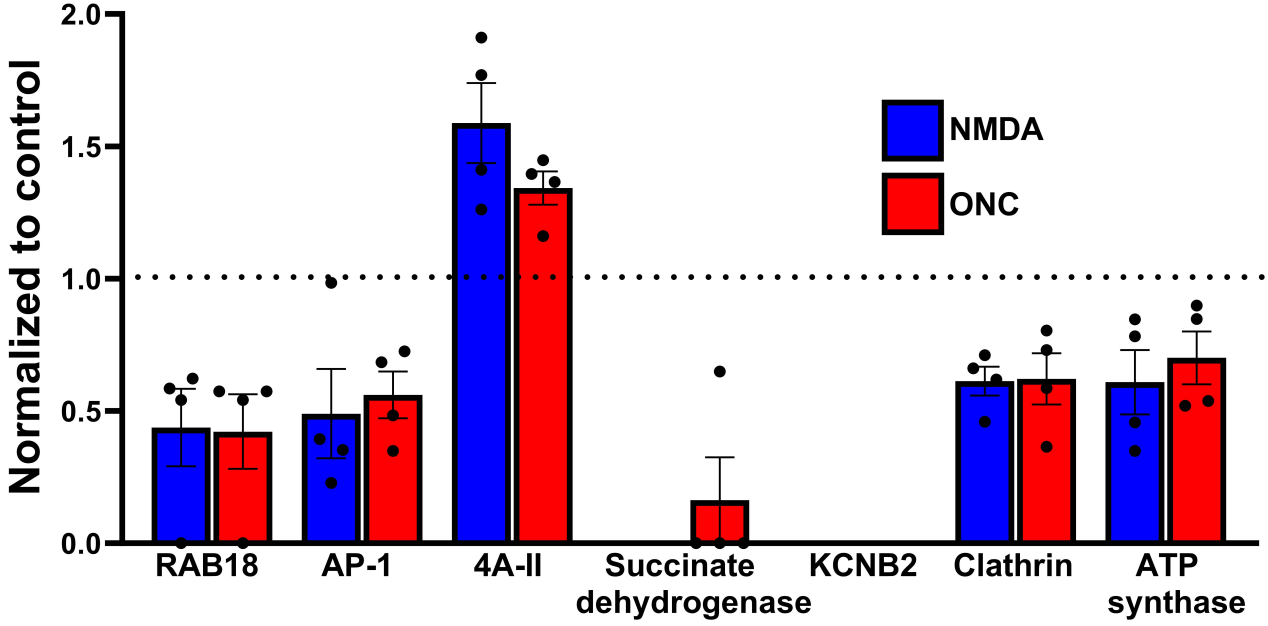
Normalized to control
2.0
1.5
1.0
0.5
0.0
NMDA
ONC
RAB18
AP-1
4A-II
Succinate dehydrogenase
KCNB2
Clathrin
ATP synthase

Table 1- Proteins differentially expressed following NMDA treatment

Protein Name	Accession Number	p-value	Level compared to control
40S ribosomal protein S10	P63325	0.011	elevated
Peptidyl-prolyl cis-trans isomerase FKBP1A	P26883	0.030	elevated
SUMO-activating enzyme subunit 1	Q9R1T2	0.001	elevated
Probable ATP-dependent RNA helicase DDX28	Q9CWT6	0.029	elevated
Metastasis-associated protein MTA2	Q9R190	0.011	elevated
6-phosphogluconolactonase	Q9CQ60	0.014	elevated
Plasminogen activator inhibitor 1 RNA-binding protein	Q9CY58	0.043	elevated
Phosducin	Q9QW08	0.020	elevated
Eukaryotic translation initiation factor 4B	Q8BGD9	0.015	elevated
DnaJ homolog subfamily C member 8	Q6NZB0	0.041	elevated
ADP-ribosylation factor-like protein 3	Q9WUL7	0.036	elevated
Hypoxanthine-guanine phosphoribosyltransferase	P00493	0.048	elevated
Inositol (Myo)-1(Or 4)-monophosphatase 1	Q924B0	0.033	elevated
DNA-(apurinic or apyrimidinic site) lyase	P28352	0.001	elevated
Ras GTPase-activating protein 4	Q6PFQ7	0.032	elevated
Lactoylglutathione lyase	Q9CPU0	0.027	elevated
Cold-inducible RNA-binding protein	P60824	0.034	elevated
Eukaryotic initiation factor 4A-II	E9Q561	0.011	elevated
Guanylate kinase	Q64520	0.042	elevated
Elongation factor 1-beta	O70251	0.039	elevated
Heterogeneous nuclear ribonucleoprotein F	Q9Z2X1	0.018	elevated
T-complex protein 1 subunit delta	P80315	0.025	elevated
14-3-3 protein epsilon	D6REF3	0.019	elevated
SUMO-activating enzyme subunit 2	Q9Z1F9	0.041	elevated
Acidic leucine-rich nuclear phosphoprotein 32 family member B	Q9EST5	0.049	elevated
Triosephosphate isomerase	P17751	0.007	elevated
Aspartate aminotransferase, cytoplasmic	P05201	0.050	elevated
Tubulin alpha-1C chain	P68373	0.035	elevated
Phosphoglycerate mutase 1	Q9DBJ1	0.029	elevated
Heterogeneous nuclear ribonucleoprotein A1	P49312	0.027	elevated
Heterogeneous nuclear ribonucleoproteins A2/B1	O88569	0.043	elevated
Small nuclear ribonucleoprotein D3	Q91VM2	0.031	elevated
CST complex subunit STN1	Q8K2X3	0.049	elevated
UMP-CMP kinase	Q9DBP5	0.043	reduced
ATP-dependent 6-phosphofructokinase, platelet type	Q9WUA3	0.035	reduced
NADH-ubiquinone oxidoreductase 75 kDa subunit, mitochondrial	Q91VD9	0.016	reduced
Aconitate hydratase, mitochondrial	Q99KI0	0.016	reduced
Inorganic pyrophosphatase	Q9D819	0.038	reduced

Table 1- Proteins differentially expressed following NMDA treatment

Sodium/potassium-transporting ATPase subunit alpha-3	Q6PIC6	0.020	reduced
Sodium/potassium-transporting ATPase subunit alpha-1	Q8VDN2	0.022	reduced
N(G),N(G)-dimethylarginine dimethylaminohydrolase 1	Q9CWS0	0.044	reduced
Voltage-dependent anion-selective channel protein 2	Q60930	0.029	reduced
Protein piccolo	Q9QYX7	0.021	reduced
Cytochrome b-c1 complex subunit 2, mitochondrial	Q9DB77	0.017	reduced
Clathrin coat assembly protein AP180	Q61548	0.021	reduced
Mitochondrial carrier homolog 2	Q791V5	0.022	reduced
ATP synthase subunit d, mitochondrial	Q9DCX2	0.020	reduced
Leucine-rich repeat-containing protein 59	Q922Q8	0.013	reduced
Dihydrolipoyllysine-residue acetyltransferase component of pyruvate dehydrogenase complex, mitochondrial	Q8BMF4	0.044	reduced
Synaptogyrin-3	Q8R191	0.032	reduced
Enoyl-CoA delta isomerase 1, mitochondrial	P42125	0.049	reduced
MICOS complex subunit Mic60	Q8CAQ8	0.031	reduced
Ras-related protein Rab-18	P35293	0.002	reduced
Protein NipSnap homolog 1	O55125	0.037	reduced
Fumarate hydratase, mitochondrial	P97807	0.009	reduced
Transportin-1	Q8BFY9	0.043	reduced
MAGUK p55 subfamily member 2	Q9WV34	0.050	reduced
Calcium-binding mitochondrial carrier protein Aralar1	Q8BH59	0.001	reduced
Cytochrome c1, heme protein, mitochondrial	Q9D0M3	0.025	reduced
Alpha-actinin-4	P57780	0.018	reduced
Succinyl-CoA ligase [ADP-forming] subunit beta, mitochondrial	Q9Z2I9	0.025	reduced
Transforming protein RhoA	Q9QUI0	0.019	reduced
Microtubule-associated protein 6	Q7TSJ2	0.010	reduced
Spna2 protein	B9EKJ1	0.030	reduced
Isocitrate dehydrogenase [NAD] subunit, mitochondrial	Q91VA7	0.048	reduced
AP-1 complex subunit beta-1	O35643	0.024	reduced
Carbonic anhydrase 14	Q9WVT6	0.012	reduced
40S ribosomal protein S3a	P97351	0.023	reduced
Pyruvate dehydrogenase E1 component subunit beta, mitochondrial	Q9D051	0.023	reduced
60S acidic ribosomal protein P0	P14869	0.014	reduced
Ornithine aminotransferase, mitochondrial	P29758	0.047	reduced
Sideroflexin-3	Q91V61	0.003	reduced
Sodium- and chloride-dependent GABA transporter 3	P31650	0.044	reduced
NADH dehydrogenase [ubiquinone] iron-sulfur protein 8, mitochondrial	Q8K3J1	0.007	reduced
Mannose-P-dolichol utilization defect 1 protein	Q9R0Q9	0.003	reduced
Catenin (Cadherin associated protein), alpha 1	Q6NV50	0.041	reduced
Importin subunit beta-1	P70168	0.046	reduced

Table 1- Proteins differentially expressed following NMDA treatment

Catenin beta-1	Q02248	0.010	reduced
Cytochrome b-c1 complex subunit Rieske, mitochondrial	Q9CR68	0.020	reduced
Pyridoxal kinase	Q8K183	0.034	reduced

Table 2- Proteins Differentially expressed following ONC

Protein Names	Accession Number	p-value Control vs ONC	Level compared to control
Splicing factor 3A subunit 1	Q8K4Z5	0.050	elevated
CST complex subunit STN1	Q8K2X3	0.028	elevated
Stomatin-like protein 2, mitochondrial	Q99JB2	0.015	elevated
DnaJ homolog subfamily C member 8	Q6NZB0	0.047	elevated
Hepatoma-derived growth factor-related protein 2	Q3UMU9	0.013	elevated
Ddx3x protein	B9EKE9	0.017	elevated
von Willebrand factor A domain-containing protein 8	Q8CC88	0.039	elevated
High mobility group protein B3	O54879	0.003	elevated
DNA-(apurinic or apyrimidinic site) lyase	P28352	0.004	elevated
Inosine-5'-monophosphate dehydrogenase 1	P50096	0.047	elevated
Peptidyl-prolyl cis-trans isomerase A	P17742	0.020	elevated
Histone H2B type 3-A	Q9D2U9	0.024	elevated
Acidic leucine-rich nuclear phosphoprotein 32 family member E	P97822	0.035	elevated
Histone H2B type 1-H	Q64478	0.024	elevated
Cullin-associated NEDD8-dissociated protein 1	Q6ZQ38	0.048	elevated
Heterogeneous nuclear ribonucleoprotein F	Q9Z2X1	0.029	elevated
Eukaryotic initiation factor 4A-II	E9Q561	0.012	elevated
Protein DEK	Q7TNV0	0.030	elevated
Ras-related protein Rab-6A	P35279	0.028	elevated
Peroxiredoxin-1	P35700	0.042	reduced
Transketolase	P40142	0.028	reduced
Dihydropyrimidinase-related protein 2	O08553	0.007	reduced
Small nuclear ribonucleoprotein D3	Q91VM2	0.013	reduced
ATP synthase subunit d, mitochondrial	Q9DCX2	0.028	reduced
Cytoplasmic dynein 1 heavy chain 1	Q9JHU4	0.045	reduced
T-complex protein 1 subunit gamma	P80318	0.037	reduced
Fumarate hydratase, mitochondrial	P97807	0.038	reduced
Actin-related protein 3	Q99JY9	0.022	reduced
Synaptotagmin-1	P46096	0.028	reduced
ATP-dependent 6-phosphofructokinase, liver type	P12382	0.008	reduced
T-complex protein 1 subunit alpha	P11983	0.021	reduced
Protein kinase, cAMP dependent regulatory, type II alpha	Q8K1M3	0.039	reduced
Clathrin coat assembly protein AP180	Q61548	0.026	reduced
Carbonic anhydrase 14	Q9WVT6	0.045	reduced
Cofilin-1	P18760	0.024	reduced

Table 2- Proteins Differentially expressed following ONC

Mitochondrial 2-oxoglutarate/malate carrier protein	Q9CR62	0.048	reduced
Ras-related protein Rab-18	P35293	0.002	reduced
Kras protein	Q5J7N1	0.027	reduced
AP-1 complex subunit beta-1	O35643	0.005	reduced
Enoyl-CoA hydratase, mitochondrial	Q8BH95	0.045	reduced
Transforming protein RhoA	Q9QUI0	0.037	reduced
Prohibitin	P67778	0.044	reduced
Transportin-1	Q8BFY9	0.040	reduced
26S proteasome non-ATPase regulatory subunit 2	Q8VDM4	0.023	reduced
Tubby-related protein 1	Q9Z273	0.042	reduced
Pyridoxal phosphate phosphatase	P60487	0.031	reduced
Protein NipSnap homolog 2	O55126	0.019	reduced
ATP-dependent 6-phosphofructokinase, muscle type	P47857	0.045	reduced
RNA-binding protein EWS	Q61545	0.018	reduced
Glycogen phosphorylase, brain form	Q8CI94	0.004	reduced
Ornithine aminotransferase, mitochondrial	P29758	0.048	reduced
Moesin	P26041	0.007	reduced
Microtubule-associated protein 6	Q7TSJ2	0.008	reduced
Catenin (Cadherin associated protein), alpha 1	Q6NV50	0.043	reduced
N(G),N(G)-dimethylarginine dimethylaminohydrolase 1	Q9CWS0	0.009	reduced
Sodium- and chloride-dependent GABA transporter 3	P31650	0.037	reduced
UMP-CMP kinase	Q9DBP5	0.008	reduced
Catenin beta-1	Q02248	0.009	reduced
Vesicle-associated membrane protein-associated protein A	Q9WV55	0.030	reduced
Protein disulfide-isomerase A4	P08003	0.044	reduced
Importin subunit beta-1	P70168	0.029	reduced

Table 3- Proteins differentially expressed in both NMDA and ONC groups

Protein Name	Accession Number	p-value control vs NMDA	p-value control vs ONC	Level-NMDA vs control	Level-ONC vs control
Ras-related protein Rab-18	P35293	0.002	0.002	reduced	reduced
DNA-(apurinic or apyrimidinic site) lyase	P28352	0.001	0.004	elevated	elevated
AP-1 complex subunit beta-1	O35643	0.024	0.005	reduced	reduced
UMP-CMP kinase	Q9DBP5	0.043	0.008	reduced	reduced
Microtubule-associated protein 6	Q7TSJ2	0.010	0.008	reduced	reduced
N(G),N(G)-dimethylarginine dimethylaminohydrolase 1	Q9CWS0	0.044	0.009	reduced	reduced
Catenin beta-1	Q02248	0.010	0.009	reduced	reduced
Eukaryotic initiation factor 4A-II	E9Q561	0.011	0.012	elevated	elevated
Small nuclear ribonucleoprotein D3	Q91VM2	0.031	0.013	elevated	reduced
Clathrin coat assembly protein AP180	Q61548	0.021	0.026	reduced	reduced
ATP synthase subunit d, mitochondrial	Q9DCX2	0.020	0.028	reduced	reduced
CST complex subunit STN1	Q8K2X3	0.049	0.028	elevated	elevated
Importin subunit beta-1	P70168	0.046	0.029	reduced	reduced
Heterogeneous nuclear ribonucleoprotein F	Q9Z2X1	0.018	0.029	elevated	elevated
Sodium- and chloride-dependent GABA transporter 3	P31650	0.044	0.037	reduced	reduced
Transforming protein RhoA	Q9QUI0	0.019	0.037	reduced	reduced
Fumarate hydratase, mitochondrial	P97807	0.009	0.038	reduced	reduced
Transportin-1	Q8BFY9	0.043	0.040	reduced	reduced
Catenin (Cadherin associated protein), alpha 1	Q6NV50	0.041	0.043	reduced	reduced
Carbonic anhydrase 14	Q9WVT6	0.012	0.045	reduced	reduced
DnaJ homolog subfamily C member 8	Q6NZB0	0.041	0.047	elevated	elevated
Ornithine aminotransferase, mitochondrial	P29758	0.047	0.048	reduced	reduced